REPORT DOCUMENTATION PAGE

Form Approved
OMB No. 0704-0188

PLEASE DO NOT RETURN YOUR FORM TO THE ABOVE ORGANIZATION.

1. REPORT DATE *(DD-MM-YYYY)*	2. REPORT TYPE	3. DATES COVERED *(From - To)*
01-02-2008	FINAL REPORT	1 September 2003 - 31 August, 2007

4. TITLE AND SUBTITLE

MICRODISCHARGES FOR PHASED ARRAYS OF LOW COHERENCE EMITTERS, AND MICROCHIP AND MICROSPHERE LASERS

5a. CONTRACT NUMBER

5b. GRANT NUMBER

F49620-03-1-0391

5c. PROGRAM ELEMENT NUMBER

6. AUTHOR(S)

DR EDEN

5d. PROJECT NUMBER

5e. TASK NUMBER

5f. WORK UNIT NUMBER

7. PERFORMING ORGANIZATION NAME(S) AND ADDRESS(ES)

UNIVERSITY OF ILLINOIS
1406 WEST GREEN STREET
URBANA, IL 61801

8. PERFORMING ORGANIZATION REPORT NUMBER

9. SPONSORING/MONITORING AGENCY NAME(S) AND ADDRESS(ES)

AF OFFICE OF SCIENTIFIC RESEARCH
875 NORTH RANDOLPH STREET ROOM 3112
ARLINGTON VA 22203
DR HOWARD SCHLOSSBERG/NE

10. SPONSOR/MONITOR'S ACRONYM(S)

11. SPONSOR/MONITOR'S REPORT NUMBER(S)

12. DISTRIBUTION/AVAILABILITY STATEMENT

DISTRIBUTION STATEMEN A: UNLIMITED

AFRL-SR-AR-TR-08-0171

13. SUPPLEMENTARY NOTES

14. ABSTRACT

Arrays as large as 250,000 Si microcavity plasma devices have been fabricated and tested extensively. Exciting a phosphor with VUV emission from these arrays yields values of the luminous efficacy > 7 lumens/W, considerably higher than that available fro conventional plasma displays. A new microplasma technology based on nanopourous Al2O3 grown on Al has been developed, and arrays with emitting areas> 20 cm2 have been demonstrated. Successfully sealed in plastic sheets, or with a thin glass or quartz window, these arrays are quite inexpensive and manufacturable by roll-to-roll processing. Shaping o fthe electric field within a microplasma has been achieved by engineering the plasma/dielectric interface.

15. SUBJECT TERMS

16. SECURITY CLASSIFICATION OF:			17. LIMITATION OF ABSTRACT	18. NUMBER OF PAGES	19a. NAME OF RESPONSIBLE PERSON
a. REPORT	b. ABSTRACT	c. THIS PAGE			19b. TELEPHONE NUMBER *(Include area code)*

FINAL REPORT FOR

AFOSR GRANT NO.

F49620-03-1-0391

"MICRODISCHARGES FOR PHASED ARRAYS OF LOW COHERENCE EMITTERS, AND MICROCHIP AND MICROSPHERE LASERS"

September 1, 2003 — August 31, 2006

Submitted to
Dr. Howard R. Schlossberg
AFOSR/NE
4th Floor, One Liberty Center
875 North Randolph Street
Arlington, VA 22203
703-696-7549

Prepared by
J. G. Eden
Laboratory for Optical Physics and Engineering
Department of Electrical and Computer Engineering
University of Illinois
1406 West Green Street
Urbana, IL 61801

February 2008

TABLE OF CONTENTS

I. Major Accomplishments Under AFOSR Grant F49620-03-1-0391

With AFOSR support under grant no. F49620-03-1-0391, our laboratory (Optical Physics and Engineering) at the University of Illinois has pursued over the past several years the physics and technology of microcavity plasma devices and arrays. This new field has enormous potential for both plasma and optical science, as well as technological applications, as evidenced by several of the advances made during the course of this grant:

1. Arrays as large as 250,000 (500 × 500) Si microcavity plasma devices have been fabricated and tested extensively. Exciting a phosphor with VUV emission (Xe_2 dimer) from these arrays yields values of the luminous efficacy > 7 lumens/W, considerably higher than that available from conventional plasma displays.

2. A new microplasma technology based on nanoporous Al_2O_3 grown on Al has been developed, and arrays with emitting areas > 20 cm^2 have been demonstrated. Successfully sealed in plastic sheets, or with a thin glass or quartz window, these arrays are quite inexpensive and manufacturable by roll-to-roll processing.

3. Fully transparent and flexible arrays of microcavity plasmas have been fabricated by replica molding techniques. Plasma channels as small as a few μm in the transverse dimension have been demonstrated which was long thought to not be possible. Uniform glow plasmas can now be confined to cavities with dimensions the same as those of a conventional single mode optical waveguide. We have also fabricated and successfully demonstrated complex optical structures such as a 150 ring Fresnel zone plate and a 1 Mpixel array.

4. Shaping of the electric field within a microplasma has been achieved by engineering the plasma/dielectric interface.

5. An extensive series of vibrational bands of the Xe dimer has been observed by laser spectroscopy. The significance of this result is that the transitions originate from the Xe_2 ($a^3\Sigma_u^+$) metastable state and are a strong candidate for enabling a molecular Anti-Stokes Raman laser (ASRL).

6. Dipole-dipole interactions between two excited atoms have been observed at long range ($250 \leq R \leq 1100$ Å) with a newly-developed spectroscopic technique on the femtosecond time scale in which a wavepacket is combined with parametric four wave mixing.

7. Thirteen patent applications have been filed with the U.S. Patent and Trademark Office, seven have been granted, and the claims for another patent have recently been allowed by the Examiner.

These are only a few of the accomplishments that were realized under this AFOSR grant. Other milestones achieved include the detection of magnetic fields as weak as 1 nT with a magnetic-optical technique operating at room temperature, and the demonstration of fully-addressable Si microplasma devices.

The next section describes in a bit more detail several of the accomplishments cited above. We are most grateful for the support of the AFOSR during this three year period and hope that the Air Force is as pleased with the advances in this technology as are we.

A. Large Arrays of Si Inverted Pyramid Microplasma Devices

We reported the first microplasma devices fabricated in Si in 1997 and, in 2001, the inverted square pyramid microcavity structure was introduced [1]. Microcavities having the form of a square cross-section trench or an inverted square pyramid have been most extensively studied to date, but the preponderance of our processing development and plasma characterization efforts have been directed towards the latter. This particular microcavity geometry was chosen for several reasons, the foremost of which is the reproducibility of the microcavity dimensions and shape (the sidewalls of the pyramid are Si(111) planes) from device to device, a crucial aspect when one is investigating the electrical and optical behavior of nanoliter volume plasmas or when contemplating the design of ultralarge arrays of microplasmas.

A cross-sectional diagram of a single Si microplasma device, designed for excitation by an AC voltage waveform (sinusoidal or bipolar), is presented by the left-hand portion of Fig. 1. The inverted pyramidal microcavity is formed by conventional wet processing of 300 μm thick Si(100) wafers and a multilayer dielectric structure provides the electrical and physical isolation of the electrodes conducive to long life of the device [2]. Devices having this design have proven to be robust and yield arrays with extraordinary emission uniformity from device-to-device. When the desired gas or vapor mixture is introduced to the microcavity of Fig. 1 and a time-varying voltage is applied between the Si substrate and the top electrode (a Au/Ni bilayer, in this case), a uniform glow discharge is produced within the microcavity and, depending upon the operating conditions, the plasma can extend above the cavity as well. This hybrid semiconductor/plasma device is characterized by the ability to produce glow discharges in gases or vapors at pressures up to and beyond one atmosphere which is a consequence of *pd* scaling

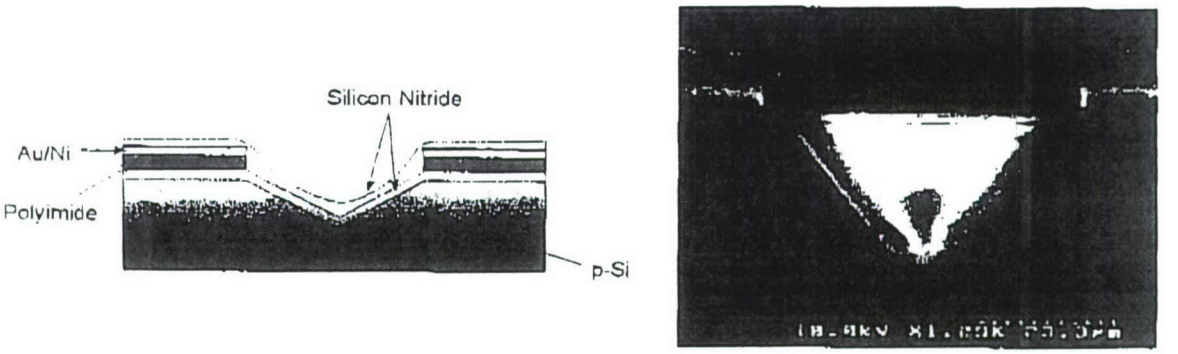

Fig. 1. (Left) Cross-sectional diagram of an inverted square pyramid microcavity device designed for AC excitation at frequencies of 5-20 kHz. The drawing is not to scale and this general design operates well with various dielectric and electrode materials; (Right) SEM of a single pyramidal device from above, showing the Si(111) sidewalls.

(where p and d are the gas pressure and characteristic dimension of the microcavity, respectively). The result is that these devices produce stable, spatially-uniform plasmas operating continuously at pressures favorable to the formation of transient (short-lived) molecules, such as the rare gas dimers and the rare gas-halides, which are known to be efficient emitters in the ultraviolet. A scanning electron micrograph (SEM) of a single Si inverted pyramid device (viewed from above) is given by the right half of Fig. 1.

Figure 2 is a photograph (acquired with a telescope and a CCD camera) of a portion of a 500×500 array — the largest array fabricated to date — of 50×50 μm^2 pyramidal Si devices [3]. Operating at a Ne gas pressure of 700 Torr and a sinusoidal AC driving frequency of 15 kHz, the array produces strong emission (luminance of several hundred cd-m^{-2}) that is uniform from device-to-device, across the entire array, to well within ±10%. Although experimentation and computational modeling remain to determine the optimal cross-section and electrode/ dielectric configuration for producing UV and/or visible emission most efficiently, it must be emphasized that the structure of Figs. 1 and 2 is the result of several years of effort invested in the testing and microfabrication processing of various device designs. This structure has a filling factor of 25%, is reliable and long-lived and, perhaps more importantly, no significant barriers to developing arrays with active areas beyond 100 cm^2 are envisioned. Furthermore, the emission uniformity evident in Fig. 2 is obtained for every array we have fabricated with the structure of Fig. 1. This technology has the distinct advantage of offering the ability to design microplasma

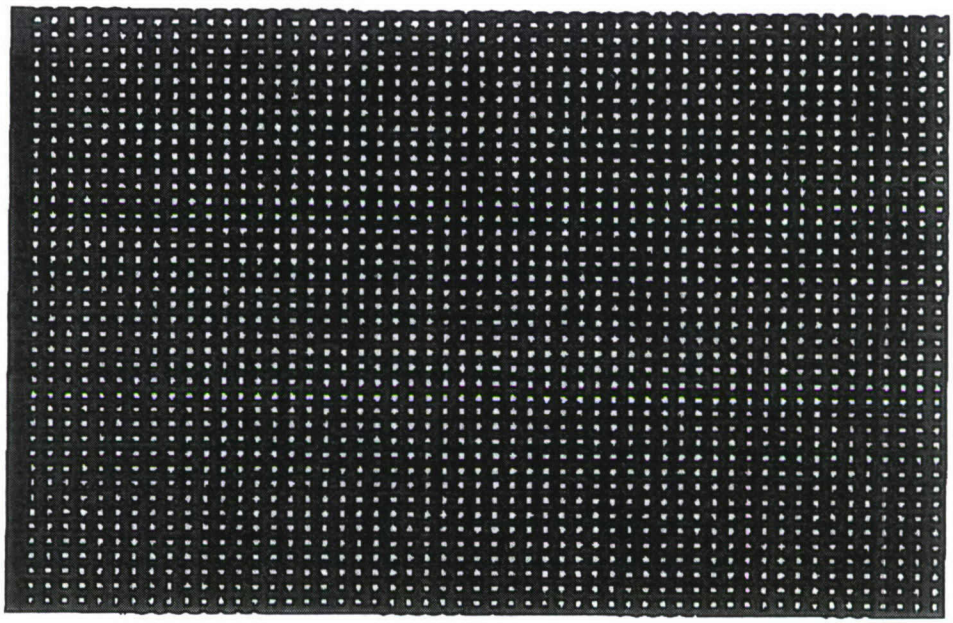

Fig. 2. Optical micrograph (recorded with a telescope and a CCD camera) of a 54 × 40 segment of a 500 × 500 array of $(50\ \mu m)^2$ Si pyramidal microcavity devices driven by a sinusoidal AC waveform having a frequency of 15 kHz. The Ne pressure is 700 Torr and the device pitch (along both orthogonal coordinates) is 100 μm [3].

emitters in Si with precision by employing well-developed microfabrication techniques. Such a capability is expected to be of considerable value in those biomedical and display applications for which interfacing the microcavity device array with electronics or other photonic devices is a significant asset.

Equally important is the radiative efficiency of these novel emitters. The size of the 500 × 500 arrays (active area of 25 cm^2) is now sufficiently large to yield reliable luminance data. Photographs of a 500 × 500 array operating in Ne and a Ne/50% Xe gas mixture are shown in Fig. 3. In both cases, the total pressure is 700 Torr and a glass plate coated with a commercial green phosphor ($Mn:Zn_2SiO_4$) covers only the upper half of the array. An uncoated glass plate is situated over the remaining half of the array. With 700 Torr of Ne in the microcavity devices (left portion of Fig. 3), predominantly visible emission is produced by the array but UV fluorescence from Ne^+ lines generates green emission from the phosphor that, when combined with transmitted red fluorescence, appears yellow to the eye. The introduction of a Ne/50% Xe mixture to the array (Fig. 3, right side), however, generates intense green emission from the phosphor as a result of vacuum ultraviolet fluorescence from both atomic Xe and Xe_2. Little visible emission is produced from the array itself.

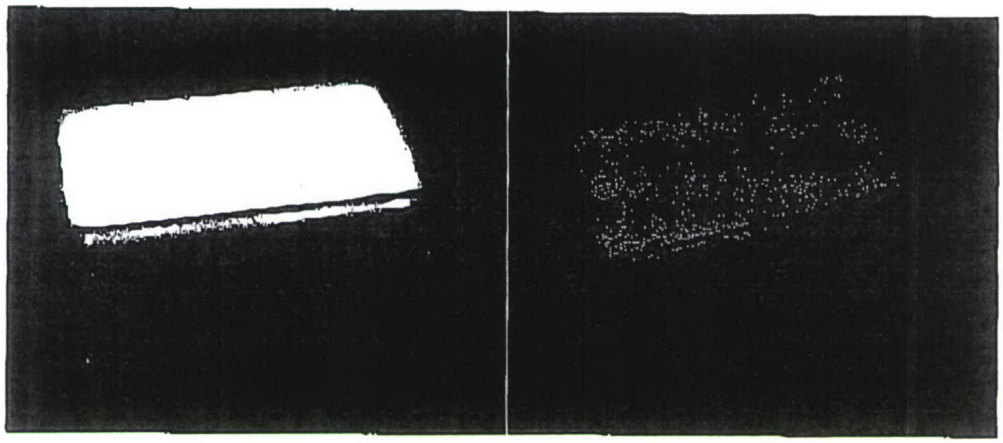

Fig. 3. Operation of the 500 × 500 array in 700 Torr of Ne (left) and in a 350 Torr Ne/350 Torr Xe mixture (right). For both photographs, a 20 μm-thick film of a green phosphor ($Mn:Zn_2SiO_4$), screen printed onto a 1 mm thick glass microscope slide, is mounted above only the upper half of the 500 × 500 array. An uncoated plate covered the remaining half of the array and the array-phosphor spacing is ≤ 2 mm.

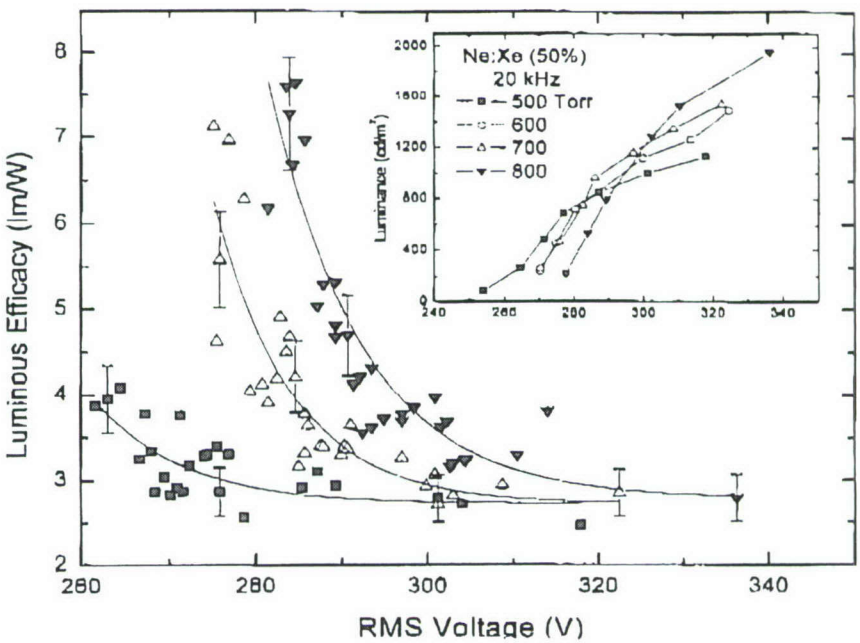

Fig. 4. Dependence of the luminous efficacy on the RMS driving voltage when a 500 × 500 array operating with Ne/50% Xe gas mixtures illuminates a film of $Mn:Zn_2SiO_4$ green phosphor screen-printed onto a glass plate. A sinusoidal ac waveform with a frequency of 20 kHz excited the array and data are presented for a total mixture pressure of 500-800 Torr. Estimated uncertainties, representative of those for all of the data, are shown for several measurements. Also, the variation of the 500 × 500 array luminance with ac excitation voltage (RMS) is illustrated by the inset. Data are again given for Ne/50% Xe gas mixtures at pressures from 500 to 800 Torr and an ac excitation frequency of 20 kHz.

Only a fraction of the data obtained to date can be discussed but Fig. 4 presents luminance and luminous efficiency results for Ne/50% Xe mixtures and a driving frequency of 20 kHz. The rapid rise in efficacy with increasing Xe partial pressure, particularly evident at lower voltages ($\leq$ 290 V RMS), is a consequence of enhanced Xe_2 formation. Notice that efficacy values above 6 lumens/W are observed for total gas pressures of 700-800 Torr and the highest observed value, 7.2 ± 0.6 lumens/W, was recorded at 800 Torr for an excitation voltage of ~284 V RMS. These results strongly suggest that the specific power loadings afforded by spatially confining the plasma to a microcavity has a beneficial impact on excimer production efficiency that will significantly impact applications such as high resolution displays. It should also be mentioned that preliminary experiments incorporating an MgO film into the microcavities (in order to raise the secondary electron emission coefficient) result in operating voltages that are 20-25% lower than those of Fig. 4.

The progress realized over the past two years in fabricating such large arrays is difficult to overstate. In a proposal submitted to AFOSR approximately five years ago, our state-of-the-art Si microplasma array was a 30 × 30 structure driven DC and requiring voltages up to 1130 V! Equally interesting was the comment made at the time concerning the spatial variation of the emission intensity: "Further improvement in the spatial uniformity of the emission produced by these large arrays is clearly necessary...and this subject is being pursued further..." These problems have now been solved and we are currently developing addressable Si devices. Applications in biomedical diagnostics and high resolution displays are of immediate priority.

B. <u>Al/Al_2O_3 Multilayer Devices: Flexible, Inexpensive Arrays</u>

One of the intriguing aspects of microcavity plasma device technology is the degree to which the inspiration for the design of single devices and arrays can draw upon, and be influenced by, advances in nanotechnology. An example is the family of robust microcavity plasma devices that we have fabricated in Al/Al_2O_3 multilayer structures by drawing upon wet chemical processing to grow thin films of nanostructured Al_2O_3 directly from the Al substrate. The chemical and optical properties of Al_2O_3, in combination with an overall device (pre-sealed) thickness of ~200 μm, make this a rugged structure that is light and flexible and yet able to withstand high power loadings.

Figure 5 is a schematic diagram of a single Al/Al_2O_3 device in cross-section. Nanoporous Al_2O_3 films 5-40 μm in thickness are grown on 127 μm thick Al foil by a multistage anodization sequence. Extensive testing has shown these films to have electrical breakdown characteristics superior to those of bulk Al_2O_3 films. A masking technique allows for 5-20 μm thick dielectric films to be grown on the interior wall of the microcavities and 20-40 μm thick on

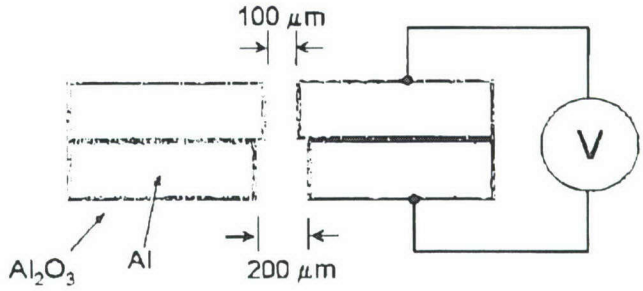

Fig. 5. Cross-sectional diagram (not to scale) of a basic Al/Al_2O_3 microplasma device structure with two conjoined cylindrical cavities.

the Al foil surface, thereby ensuring the formation of plasma within the microcavity and the absence of electrical breakdown elsewhere.

An optical micrograph of a portion of a 3 × 3 array of 250 μm dia. Al/Al_2O_3 devices is shown on the left side of Fig. 6. Notice that the dielectric film lining the interior of each microcavity is visible as a light color ring. The right half of Fig. 6 is a scanning electron micrograph (SEM) of a portion of the Al_2O_3 film surface. Each of the tips shown is situated adjacent to one of the corners of the hexagonal cross-section pores in the film.

For both the rare gases and Ar/N_2 mixtures, bright, azimuthally-uniform discharges are produced in each microcavity without the need for external ballast. The 100 μm/200 μm devices of Fig. 5 operate stably in the 400-800 Torr pressure interval, and the voltage-current (V-I) characteristics indicate that these structures prefer to operate in the abnormal glow mode. Measurements of the displacement current for a sinusoidal ac driving frequency of 10 kHz show the equivalent capacitance of a 3 × 3 array of 100 μm/200 μm devices to be ~100 pF.

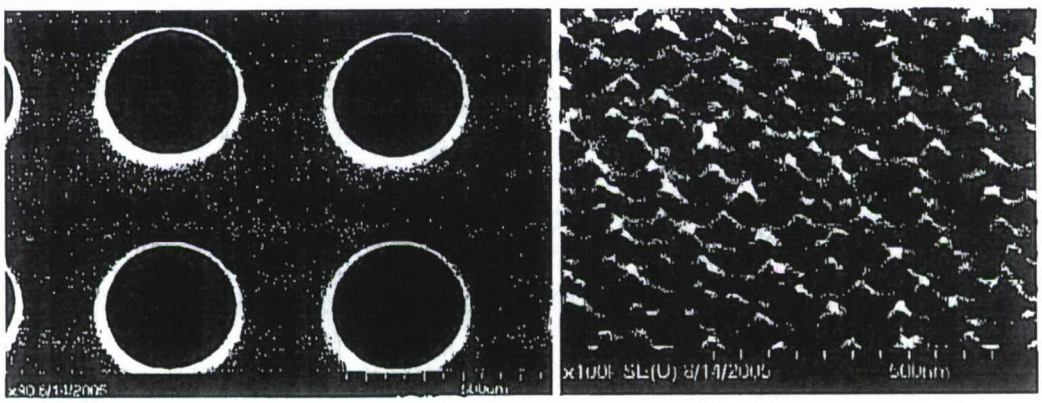

Fig. 6. (Left) Microphotograph of a segment of an array of Al/Al_2O_3 devices. The Al_2O_3 film lining the interior of each microcavity is clearly visible. (Right) SEM of a portion of the Al_2O_3 film surface.

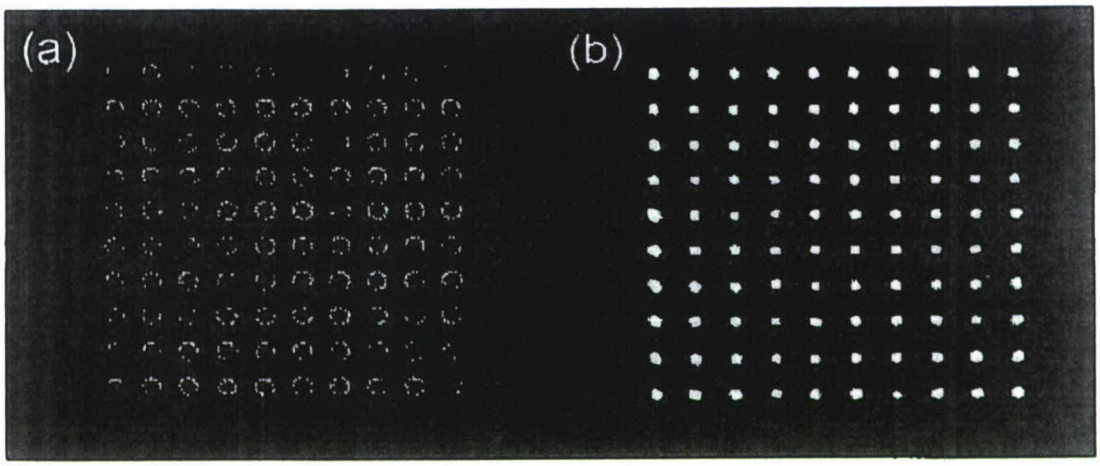

Fig. 7. Optical micrographs of a 10 × 10 array of 100 μm/200 μm Al/Al_2O_3 microplasma devices operating in 500 Torr of Ne. The RMS voltage driving the array is 198 V for image **(a)** and 226 V for **(b)**. To prevent saturation of the CCD camera, the image on the right side was recorded with a neutral density filter between the array and camera.

Microphotographs of a 10 × 10 array of 100 μm/200 μm devices, operating in 500 Torr of Ne and viewed from the 200 μm side, are presented in Fig. 7. For low levels of power deposition (left-hand portion of Fig. 7), the plasma resides almost entirely in the larger (200 μm dia.) cavity, although the electron density is concentrated at the perimeter of the cylindrical cavity. As the current to the array is increased, however, the rise in electron density is coupled with declining values of λ_D and the width of the cathode fall region. Eventually, the latter parameter becomes commensurate with (but less than) 100 μm, and the *smaller* cylindrical cavity is then able to accommodate the plasma. As illustrated by the photograph in the right half of Fig. 7, a bright core of emission is formed in each device and significant levels of radiated power are produced. As an example, unoptimized Ar/3% N_2 gas mixtures generate several tenths of a watt of near-UV (300-400 nm) power per cm^2 of array area.

Recent experiments have characterized the device structure illustrated in cross-section in Fig. 8. This design differs from that of Fig. 5 in that microcavities are produced in only one of the two electrodes, both of which are fabricated from Al foil and sealed in a 7 μm thick, nanoporous Al_2O_3 film. Part (a) of Fig. 9 is a microphotograph of a small portion of an array of Al/Al_2O_3 devices fabricated from 25 μm thick Al foil into which diamond-shaped cavities have been punched mechanically. Arrays of the design of Fig. 8, having a total thickness of 125 μm and radiating areas as large as 20 cm^2, have already been made and Fig. 9(b) is a photograph of a 7 × 2 cm^2 array operating in 700 Torr of Ne. The potential applications of this structure are (we believe) quite broad because of its scalability in area (presently limited by the size of our wet

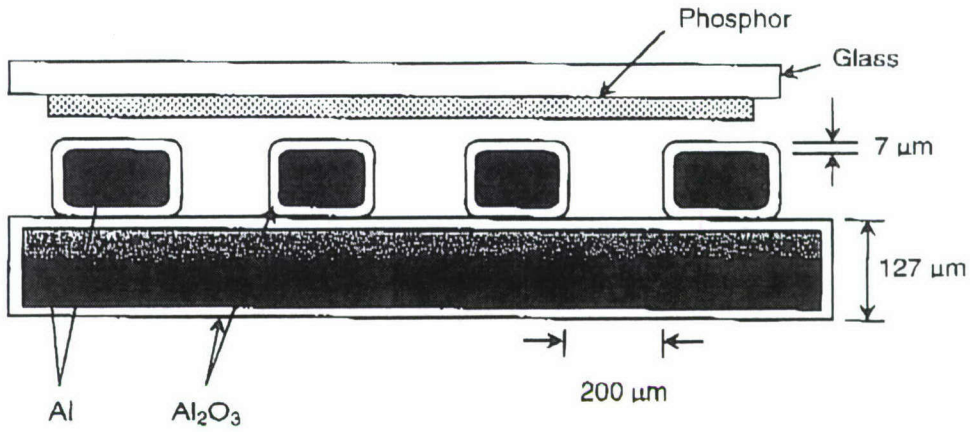

Fig. 8. Diagram (in cross-section) of a portion of an Al/Al_2O_3 microplasma array structure in which microcavities 200 μm in diameter are produced in one electrode. For several experiments, a 10 μm thick film of $Mn:Zn_2SiO_4$ green phosphor, screen-printed onto a glass plate, was mounted ~500 μm above the array.

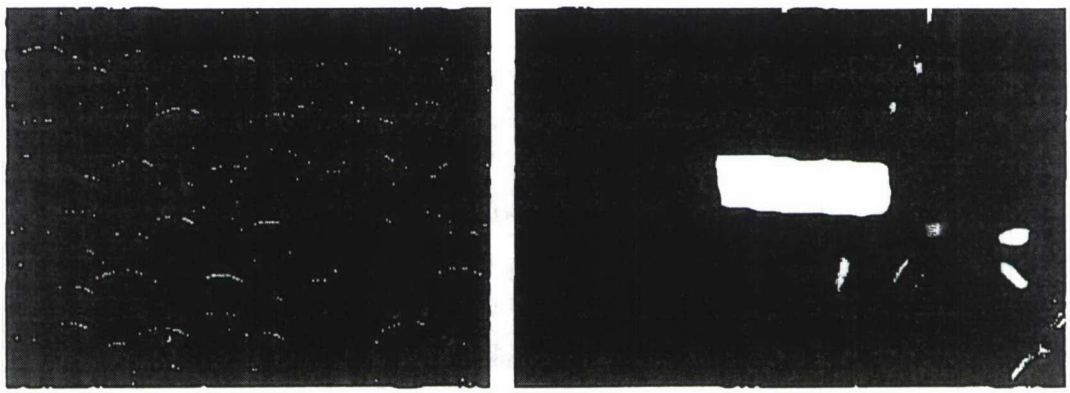

Fig. 9. (a) Microphotograph of a segment of an Al/Al_2O_3 array fabricated in 25 μm thick Al foil with diamond-shaped cavities. The array is operating in Ne at 400 Torr; (b) Photograph of a 7 cm × 2 cm rectangular array of the same structure as that in part (a). Thin glass windows are epoxied onto the array to allow it to operate outside a vacuum system. The total thickness of this array is 250 μm.

chemical processing baths). In particular, the flexibility of the arrays (when sealed by thin polymer windows) in combination with the low cost of materials and fabrication make this structure of interest for biomedical and photochemical applications requiring inexpensive, large area (hundreds of cm^2) sources. In this regard, we are collaborating with Dr. Rox Anderson of

Harvard Medical School (and Massachusetts General Hospital) and PhotoMedex to produce arrays suitable for treatment of psoriasis and actinic keratosis.

C. Ceramic Microplasma Devices with Coplanar Electrodes: Shaping the Intracavity Electric Field

We have recently succeeded in powering linear arrays of cylindrical microcavity devices, fabricated in ceramic, with buried coplanar electrodes [4]. Although ceramic-based, multilayer microplasma structures have been built and tested by our laboratory in the past, this is a much more promising design for several reasons. The foremost of these is that the intracavity electric field can be shaped by the cross-sectional geometry of the microcavity, the ceramic's dielectric constant, and the electrode spacing. Figure 10 shows top and end-on views of linear arrays of microplasma devices driven by coplanar electrodes buried in ceramic. Fabricated from low temperature cofired ceramic (LTCC) having a relative dielectric constant of 40, these devices have cylindrical microcavities with diameters of either 127 or 180 μm. The gap between the parallel Ag electrodes is fixed at 220 μm, irrespective of the diameter of the microcavities in the array.

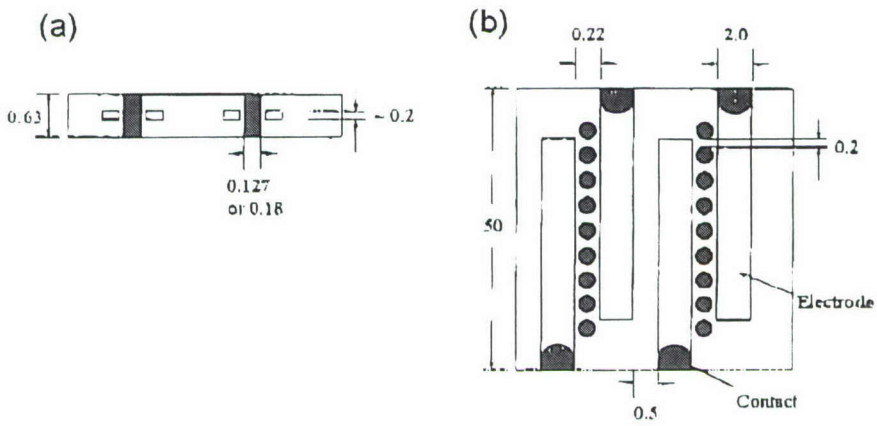

Fig. 10. Schematic diagrams (not to scale) of **(a)** end-on, and **(b)** top views of two parallel, linear arrays of cylindrical microcavity plasma devices fabricated in ceramic (LTCC). Both arrays comprise 72 microcavities (for clarity, only seven are shown) having diameters of 127 μm or 180 μm. All dimensions are expressed in mm and the separation between the inner edges of the silver electrodes is fixed at 220 μm, irrespective of the microcavity diameter.

In this geometry, curvature has been introduced into the plasma/dielectric interface, thereby distinguishing this design from most previous microplasma devices which generally sought to

optimize the azimuthal symmetry of the plasma. Figure 11 presents data showing the spatial variation of the visible radiation produced in 180 μm dia. devices operating at Ne pressures of 400 and 800 Torr. The false color images on the right side of Fig. 11(a) were recorded for p_{Ne} = 400 Torr, and the lower of the two images was obtained under conditions identical to those for

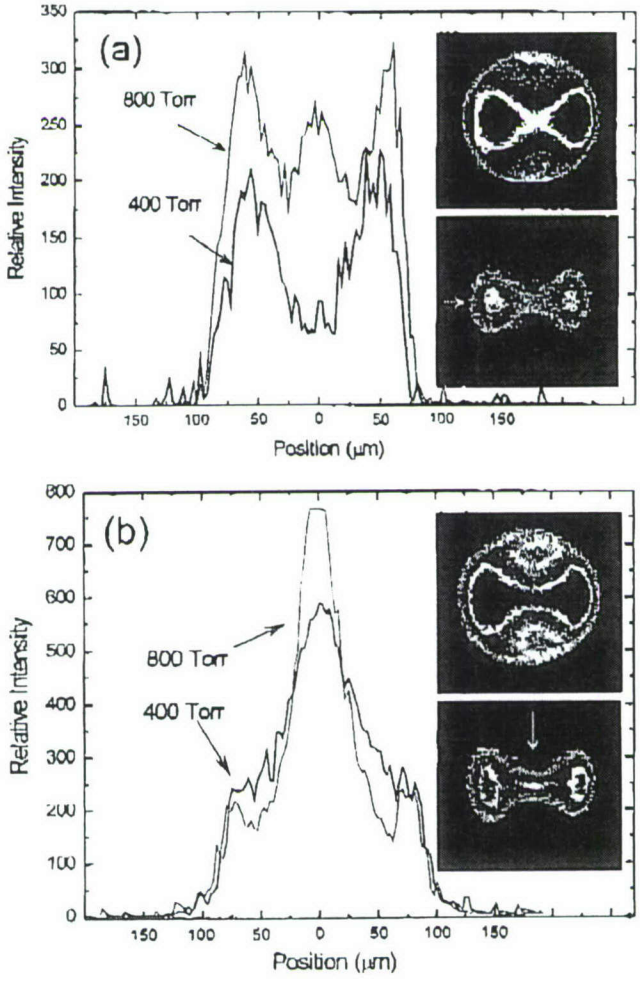

Fig. 11. Spatially resolved emission produced in 180 μm dia. microcavities: **(a)** false color images (at right) obtained at p_{Ne} = 400 Torr. The lower of the two images was recorded by attenuating the emission with a neutral density filter. On the left side, lineouts obtained in the longitudinal direction (the primary axis of the microplasma) at 400 Torr and 800 Torr are compared. The scanning direction for the lineouts is indicated by the white arrow at lower right of the figure; **(b)** false color images similar to those if part (a), but for p_{Ne} = 800 Torr, are shown on the right side. The lineouts at left illustrate the intensity profiles when scanning in the direction transverse to the discharge axis (as indicated by the white arrow).

the top image except that the intensity reaching the CCD camera was attenuated by a neutral density filter. Note that the buried electrodes (positions not indicated in Fig. 11) are oriented vertically. Emission intensity lineouts for p_{Ne} = 400 and 800 Torr are compared in the left half of Fig. 11(a). Both lineouts were obtained by scanning the digital images longitudinally — i.e., along the primary axis of the discharge indicated by the white arrow at lower right in Fig. 11(a). Similar data are given in part (b) of Fig. 11. In this case, however, the false color images on the right side were recorded for 800 Torr of Ne and the lineouts at left are associated with a vertical (transverse) scan through the emission images, as indicated by the white arrow.

The general characteristics of the microplasma emission intensity profile along the longitudinal coordinate (Fig. 11(a)) are similar to those predicted on the basis of a fluid model developed by Boeuf et al. [5] for a microplasma device in which the electrode structure and resulting plasma are azimuthally symmetric. In particular, the appearance of the central peak at 800 Torr confirms the existence of a positive column which is fully consistent with theory [5]. In the transverse direction (Fig. 11(b)), the intensity profiles reveal the presence of sidelobes that become more pronounced with increasing Ne pressure. These secondary features appear to arise from weak sheath regions established by the small transverse component of the electric field which, in turn, is introduced by the curvature of the dielectric wall at the perimeter of the microcavity. One concludes, therefore, that the combination of parallel driving electrodes and the small radius of curvature of the microcavity walls allow one partial control over the spatial variation of the electric field in the microcavity and the resulting emission intensity profile. The ability to shape the geometry of the plasma within the microcavity, while maintaining a stable glow holds considerable promise for optimizing atomic and molecular emissions from microcavities by tailoring the power loading to a specific emitting species.

D. Microplasmas Generated Within Microimprinted Cavities and Channels

Realizing the full potential of microcavity plasmas, particularly with regard to optical applications and reaching the d = 1 μm milestone, will require fabrication processes capable of inexpensively producing microcavities, and the associated electrode/dielectric structures, having precisely controlled dimensions. Furthermore, a drawback of the approaches demonstrated to date (such as those described earlier) — the difficulty of fabricating cavities (such as channels) with a high aspect ratio — must be overcome. In collaboration with Prof. B. Cunningham (UIUC), we have demonstrated the feasibility of achieving both goals with a plastic-based micromolding process of which cavities as small as $(20\ \mu m)^2$ in cross-section have been produced. By adopting a process developed for chemical, biochemical, and cell analysis sensors [6], microcavity plasmas can be generated in virtually any geometric pattern and plasma channels with aspect ratios of 10^4:1 have realized to date. A representative microcavity plasma

structure fabricated by micromolding is illustrated in cross-section in Fig. 12. The substrate is a plastic material such as polyester (PET), although other materials such as polycarbonate and PMMA may also be used. The substrate is coated with a thin film of transparent conducting material, such as indium tin oxide (ITO), which will form the bottom electrode of a microplasma device. The microcavities are formed with a micromolding process in which a "master" mold template, containing a negative volume image of the desired microcavity shape, is produced by conventional photolithography and etching of a substrate. A master mold may be produced from

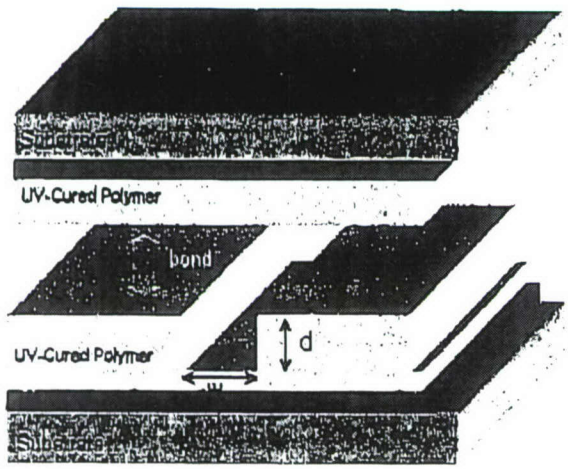

Fig. 12. Generalized diagram of a microcavity plasma structure fabricated by replica molding.

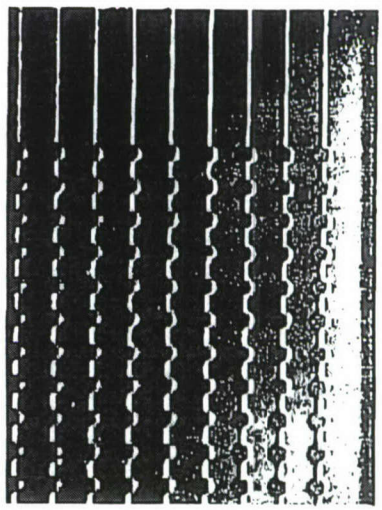

Fig. 13. Optical micrograph of an array of microcavities, ~190 μm in diameter and ~76 μm in depth. The cavities are connected by 20 μm square channels.

any durable material, including Si, glass, ceramic, or metal. To produce the microcavity array, a layer of liquid, UV-curable polymer material is squeezed between the mold and the substrate and, subsequently, cured at room temperature is ~10-90 seconds. Following the microcavity replication process, the cavities are coated with one or more dielectrics, such as TiO_2 or silicon nitride. One motivation for this step is to block vapors produced by outgassing of the polymer from entering the microcavity. Fabrication of the device of array is completed by bonding a cover (which can also be PET, as indicated in Fig. 12, or a more robust, UV-transmitting material such as glass or quartz) to the remainder of the structure. This can be accomplished by a variety of processes such as adhesive bonding, laser welding or ultrasonic welding. It must be emphasized that the replica molding process is capable of accurately reproducing features over a wide size range, from tens of nm to hundreds of μm.

Over the last eight months of the period of this grant, we fabricated and tested several microcavity device and array structures in an effort to determine the feasibility of this approach. From the first array constructed, all worked well and a few examples are presented here. Figure 13 is an optical micrograph of an array of cylindrical microcavities, ~190 μm in diameter and ~76 μm in depth, fabricated in a structure similar to that of Fig. 12. A photograph of a 20 × 20 array of these microcavities operating in 700 Torr Ne, is shown in Fig. 14 and Fig. 15 is a magnified view of the array. Not only are microplasmas produced in the 190 μm dia. cavities but, if desired, also in the 20 μm gas channels associated with each linear array. By controlling the driving voltage

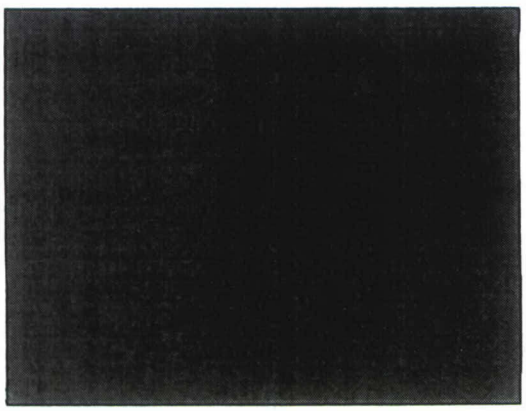

Fig. 14. Photograph of a 20 × 20 array of 190 μm dia. microcavity plasmas operating in 700 Torr of He. Under these conditions, the 20 μm gas channels associated with each of the linear arrays are also excited.

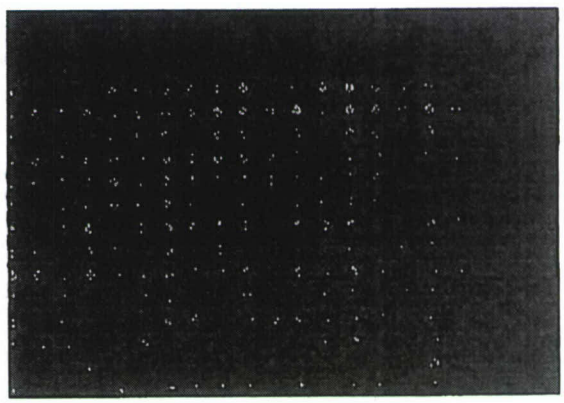

Fig. 15. Magnified view of a portion of an array similar to that of Fig. 14 but operating in Ne.

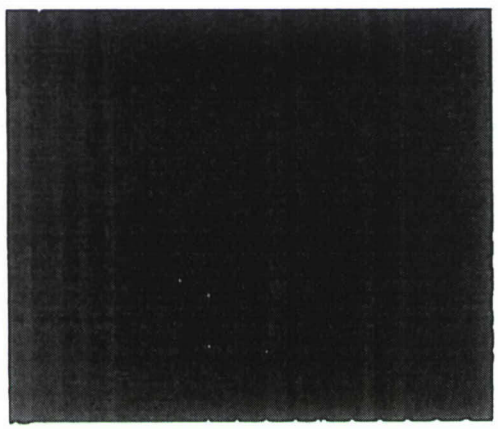

Fig. 16. Array of 20 μm plasma channels for a Ne pressure of 600 Torr.

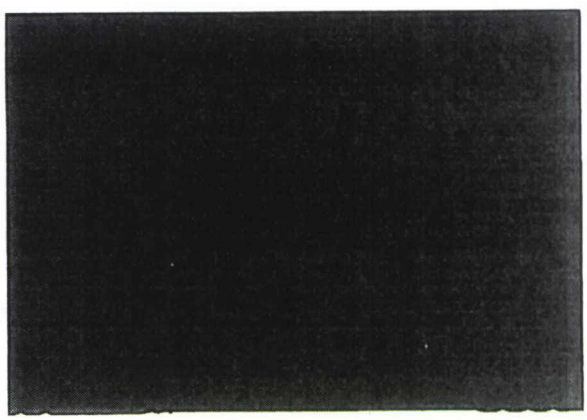

Fig. 17. Microphotograph of a single, folded 20 μm plasma channel.

magnitude and frequency, the plasma can be confined exclusively to the larger cavities or the gas channels. The ability to produce glow discharges in the flow channels was a surprise and Fig. 16 is a CCD image of an array consisting solely of plasma channels with 20×20 μm^2 cross-sections. It is clear in Fig. 16 that plasma channels having cross-sectional dimensions approaching those for single mode optical waveguides are now available. This represents an enormous asset insofar as optical probing is concerned.

A distinct advantage of producing microcavities by replica molding is the relative ease with which intricate geometric patterns can be formed, and Fig. 17 illustrates the production of nonequilibrium plasmas in Ne (at roughly atmospheric pressure) in a folded plasma channel.

To summarize, it is not an overstatement to say that the devices of Figs. 13-16 (and the associated technology) represent a new capability in the optical and plasma sciences. Plasma channels having aspect ratios up to 10^4:1 (Fig. 17) have already been realized, a value that is simply unattainable for any macroscopic plasma device. The mere fact that plasma can be confined in cavities of such small cross-section is also a surprise and suggests that plasmas of still smaller transverse dimensions can be realized. The implications of this new technology for a wide array of applications are profound and, as one final example, Fig. 18 is a photograph of a 250×250 (62,500 devices) array fabricated in PET (plastic) by the replica molding process and operating in Ne. The array is flexible and the $20 bill behind the array confirms that the array is also fully transparent.

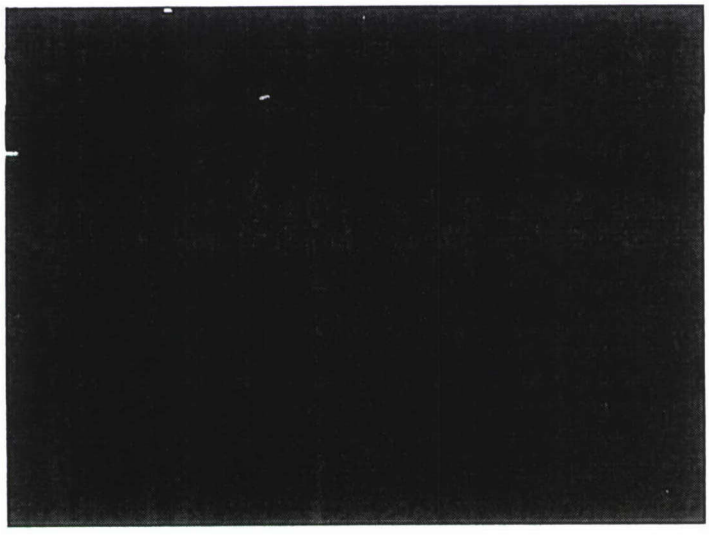

Fig. 18. Photograph of a 250×250 array of 200 μm dia. microcavities fabricated in a flexible, transparent polymer structure by replica molding. A $20 bill behind the array can clearly be seen.

E. Laser Spectroscopy: Xe_2 Rydberg States

During the course of this grant, exciting results were also been obtained in our laser spectroscopic experiments but, in the interest of brevity, only those pertaining to studies of the Rydberg states of Xe_2 will be mentioned here. The motivation for this work is the potential for demonstrating an efficient, high peak power laser in the deep UV or XUV by stimulated electronic Raman scattering. Designing an anti-Stokes Raman laser (ASRL) in a molecule is a challenge, however, because frequently the electronic excited states to be involved in the anti-Stokes process are poorly characterized. It is no surprise, then, that although more than a half-dozen atomic ASRLs were demonstrated in the late 1970s and early 1980s, no molecular ASRLs exist at present.

For several reasons that will not be elaborated here, Xe_2 is a strong candidate for an ASRL and we have, for the past two years, been studying the gerade electronic states of Xe_2 lying above the $a^3\Sigma_u^+(1_u, 0_u^-)$ metastable level. Recently, we observed extensive band structure in the near-IR (680-800 nm) in fluorescence suppression experiments monitoring the Xe_2 $(0_u^+ \rightarrow 0_g^+)$ VUV fluorescence. The measurements were made with a scanning dye laser and the result is illustrated in Fig. 19. Analysis of the vibrational bands shows the upper state responsible for these structures to be a gerade level lying ~12,400 cm^{-1} above $a^3\Sigma_u^+$ and for which R_e = 3.5 Å. Experiments show that depleting the $a^3\Sigma_u^+$ population by 30-40% when driving the transitions of Fig. 19 is straightforward and the absorption cross-sections are ~10^{-17} cm^2. These parameters are ideal for a molecular ASRL.

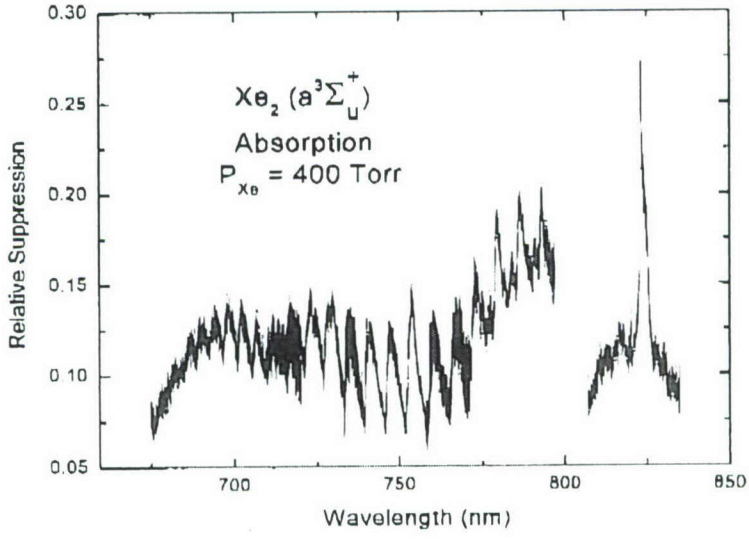

Fig. 19. Xe_2 absorption spectrum in the ~680-830 nm region obtained by fluorescence suppression spectroscopy. The absorption cross-sections for the strongest features are ~10^{-17} cm^2.

F. Summary

This section has described several of the advances in microcavity plasma devices and spectroscopy that have been realized under AFOSR grant no. F49620-03-1-0391. Large arrays of microplasma devices can now be fabricated with radiating areas > 20 cm^2 and scaling to the hundreds of cm^2 level appears to be feasible. Optical probing of d = 50-200 μm structures has revealed interesting phenomena with regard to the plasma sheath and we expect the process of elucidating microplasma physics will accelerate as we move below $d \sim 5$ μm and improve our optical probing capabilities. Of equal importance are the opportunities for applications in microlaser arrays, photomedicine, and chemical reactors on a chip.

REFERENCES

1. J. W. Frame, D. J. Wheeler, T. A. DeTemple, and J. G. Eden, *Appl. Phys. Lett.* **71**, 1165 (1997).
2. S.-J. Park, K.-F. Chen, N. P. Ostrom, and J. G. Eden, *Appl. Phys. Lett.* **86**, 111501 (2005).
3. K.-F. Chen, N. P. Ostrom, S.-J. Park, and J. G. Eden, *Appl. Phys. Lett.* **88**, 061121 (2006).
4. S.-J. Park, T. M. Spinka, and J. G. Eden, *Appl. Phys. Lett.*, **89**, 031502 (2006).
5. J. P. Boeuf, L. C. Pitchford, and K. H. Schoenbach, *Appl. Phys. Lett.* **86**, 071501 (2005).
6. B. T. Cunningham, J. Qiu, P. Li, J. Pepper, and B. Hugh, *Sensors and Actuators B* **85**, 219 (2002).

II. PAPERS PUBLISHED UNDER AFOSR SUPPORT (2003-2006)

1. P. von Allmen, S. T. McCain, N. P. Ostrom, B. A. Vojak, J. G. Eden, F. Zenhausern, C. Jensen and M. Oliver, "Ceramic microdischarge arrays with individually ballasted pixels," *Appl. Phys. Lett.*, vol. 82, pp. 2562-2564, April 21, 2003.

2. S.-J. Park and J. G. Eden, "Electrical characteristics and lifetimes of microdischarge devices having thin dielectric films of aluminum oxide, boron nitride, or barium titanate," *Electron. Lett.*, vol. 39, pp. 773-775, May 15, 2003.

3. P. von Allmen, D. J. Sadler, C. Jensen, N. P. Ostrom, S. T. McCain, B. A. Vojak, and J. G. Eden, "Linear, segmented microdischarge array with an active length of ~1 cm: cw and pulsed operation in the rare gases and evidence of gain on the 460.30 nm transition of Xe^+," *Appl. Phys. Lett.*, vol. 82, pp. 4447-4449, June 23, 2003.

4. A. A. Senin, H. C. Tran, J. Gao, Z. H. Lu, C. J. Zhu, A. L. Oldenburg, J. R. Allen, and J. G. Eden, "Molecular dissociation observed with an atomic wavepacket and parametric four-wave mixing," *Chem. Phys. Lett.*, vol. 381, pp. 53-59, November 2003.

5. J. G. Eden, S.-J. Park, N. P. Ostrom, S. T. McCain, C. J. Wagner, B. A. Vojak, J. Chen, C. Liu, P. von Allmen, F. Zenhausern, D. J. Sadler, C. Jensen, D. L. Wilcox, and J. J.

Ewing, "Microplasma devices fabricated in silicon, ceramic, and metal/polymer structures: arrays, emitters, and photodetectors," *J. Phys. D*, vol. 36, pp. 2869-2877, November 2003 (Invited).

6. B. A. Knecht, R. D. Fraser, D. J. Wheeler, C. J. Zietkiewicz, A. A. Senin, L. D. Mikheev, V. S. Zuev, and J. G. Eden, "Optical pumping of the XeF(C→A) and iodine 1.315 μm lasers by a compact surface discharge system," *Opt. Eng.*, vol. 42, pp. 3612-3621, December 2003.

7. Y.-Y. Gu, A. M. Chojnacki, C. J. Zietkiewicz, A. A. Senin, and J. G. Eden, "Autoionization in I and I_2 observed by multiphoton ionization and photoelectron spectroscopy: Two atomic iodine Rydberg series built on the $...5s^2\ 5p^4\ ^3P_1$ ion core and revised value for the $I^+(^3P_1)$ limit," *J. Chem. Phys.*, vol. 119, pp. 12342-12350, December 15, 2003.

8. G. A. Kumar, A. Martinez, E. Mejia, and J. G. Eden, "Fluorescence and upconversion spectral studies of Ho^{3+} in alkali bismuth gallate glasses," *J. Alloys and Compounds*, vol. 365, pp. 117-120, 2004.

9. Z. H. Lu, C. J. Zhu, A. A. Senin, J. R. Allen, J. Gao, and J. G. Eden, "Production and probing of atomic wavepackets with ultrafast laser pulses: Applications to atomic and molecular dynamics," *IEEE J. Sel. Topics Quantum Electron.*, vol. 10, pp. 159-168, January/February 2004.

10. S.-J. Park, K.-H. Park, and J. G. Eden, "Integration of carbon nanotubes with microplasma device cathodes: Reduction in operating and ignition voltages," *Electron. Lett.*, vol. 40, pp. 563-564, April 29, 2004.

11. J. M. Talmadge, J. Gao, M. P. Riley, R. J. Roth, S.-O. Kim, J. G. Eden, F. A. Pudonin, and I. V. Mel'nikov, "Magneto-optical Kerr effect in Fe_{21} Ni_{79} films on Si(100): Quantum behavior for film thicknesses below ~6 nm," *Appl. Phys. Lett.*, vol. 84, pp. 4197-4199, May 24, 2004.

12. S.-J. Park, J. G. Eden, and K.-H. Park, "Carbon nanotube-enhanced performance of microplasma devices," *Appl. Phys. Lett.*, vol. 84, pp. 4481-4483, May 31, 2004; also published in *Virtual J. Nanoscale Sci. Technol.*, vol. 9, May 24, 2004.

13. N. P. Ostrom, B. A. Vojak, and J. G. Eden, "Radio frequency (10-23 MHz)-assisted excitation of a microdischarge with a piezoelectric transformer," *Plasma Sources Sci. Technol.*, vol. 13, pp. 278-281 (May 2004).

14. J. G. Eden, "High order harmonic generation and other intense optical field-matter interactions: Review of recent experimental and theoretical advances," *Progress in Quantum Electronics*, vol. 28, pp. 197-246, 2004 (Invited paper).

15. R. S. Moss, J. G. Eden, and M. J. Kushner, "Avalanche processes in an idealized lamp: I. Measurements of formative breakdown time," *J. Phys. D: Appl. Phys.*, vol. 37, pp. 2502-2509 (2004).

16. M. L. Ginter and J. G. Eden, "Rydberg states of the rare gas dimers," *Can. J. Chem.*, vol. 82, pp. 762-778 (2004) — *Festschrift* issue in honor of G. Herzberg.

17. S.-J. Park, J. G. Eden, J. Chen, and C. Liu, "Microdischarge devices with 10 or 30 μm square silicon cavities: *pd* scaling and production of the XeO excimer," *Appl. Phys. Lett.*, vol. 85, pp. 4869-4871, November 22, 2004; also published in *Virtual J. Nanoscale Sci. Technol.*, vol. 10, December 6, 2004.

18. S.-J. Park, K.-F. Chen, N. P. Ostrom, and J. G. Eden, "40,000 pixel arrays of ac-excited silicon microcavity plasma devices," *Appl. Phys. Lett.*, vol. 86, 111501, March 14, 2005.

19. S.-J. Park, K.-F. Chen, N. P. Ostrom, and J. G. Eden, "Arrays of AC-excited, silicon microdischarge devices as large as 40,000 (200 × 200) pixels: electrical and optical characteristics for operation in neon," *Electron. Lett.*, vol. 41, pp. 311-312, March 17, 2005.

20. J. H. Cho, K.-W. Lee, S.-J. Park, and J. G. Eden, "Coplanar ac discharges between cylindrical electrodes with a nanoporous alumina dielectric: Modular dielectric barrier plasma devices," *IEEE Trans. Plasma Sci.*, vol. 33, pp. 378-379, April 2005.

21. S.-O. Kim and J. G. Eden, "Arrays of square cross-section microdischarge devices fabricated in glass and driven by interdigitated electrodes," *IEEE Trans. Plasma Sci.*, vol. 33, pp. 566-567, April 2005.

22. C. J. Wagner and J. G. Eden, "Xenon microdischarge at 300-800 Torr: Laser spectroscopy of Xe_2 $a^3\Sigma_u^+\left(1_u, 0_u^-\right)$," *IEEE Trans. Plasma Sci.*, vol. 33, pp. 568-569, April 2005.

23. S.-J. Park and J. G. Eden, "Stable microplasmas in air generated with a silicon inverted pyramid plasma cathode," *IEEE Trans. Plasma Sci.*, vol. 33, pp. 570-571, April 2005.

24. S.-J. Park and J. G. Eden, "Microdischarge devices with a nanoporous Al_2O_3 dielectric: Operation in Ne and air," *IEEE Trans. Plasma Sci.*, vol. 33, pp. 572-573, April 2005.

25. N. P. Ostrom and J. G. Eden, "Visible emission contours for neon plasmas in silicon microcavity discharge devices: Pressure dependence of spatially resolved fluorescence above the anode plane," *IEEE Trans. Plasma Sci.*, vol. 33, pp. 576-577, April 2005.

26. N. P. Ostrom and J. G. Eden, "Visible and near-ultraviolet emission characteristics of Ne, Ar, and Ar/N_2 excited in silicon microcavity discharge arrays," *IEEE Trans. Plasma Sci.*, vol. 33, pp. 578-579, April 2005.

27. J. G. Eden, S.-J. Park, N. P. Ostrom, and K.-F. Chen, "Recent advances in microcavity plasma devices and arrays: a versatile photonic platform," *J. Phys. D: Appl. Phys.*, vol. 38, pp. 1644-1648, 2005.

28. S.-J. Park, K. S. Kim, and J. G. Eden, "Nanoporous alumina as a dielectric for microcavity plasma devices: Multilayer Al/Al_2O_3 structures," *Appl. Phys. Lett.*, vol. 86, 221501, May 30, 2005.

29. V. S. Zuev, A. V. Frantsesson, J. Gao, and J. G. Eden, "Enhancement of Raman scattering for an atom or molecule near a metal nanocylinder: Quantum theory of spontaneous emission and coupling to surface plasmon modes," *J. Chem. Phys.*, vol. 122, 214726, June 1, 2005; also selected for publication in *Virtual J. Ultrafast Sci.*, vol. 4, July 2005.

30. S.-O. Kim and J. G. Eden, "Arrays of microplasma devices fabricated in photodefinable glass and excited AC or DC by interdigitated electrodes," *IEEE Photon. Technol. Lett.*, vol. 17, pp. 1543-1545, July 2005.

31. C.-J. Zhu, A. A. Senin, Z.-H. Lu, J. Gao, Y. Xiao, and J. G. Eden, "Polarization of signal wave radiation generated by parametric four-wave mixing in rubidium vapor: Ultrafast (~150 fs) and nanosecond time scale excitation," *Phys. Rev. A*, vol. 72, 023811, August 2005; also selected for publication in *Virtual J. Ultrafast Sci.*, vol. 4, no. 9, September 2005.

32. J. G. Eden, S.-J. Park, N. P. Ostrom, K.-F. Chen, and K. S. Kim, "Large arrays of microcavity plasma devices for active displays and backlighting," *IEEE/OSA J. Display Technol.*, vol. 1, pp. 112-117, September 2005 (Invited).

33. N. P. Ostrom and J. G. Eden, "Microcavity plasma photodetectors: Photosensitivity, dynamic range, and the plasma-semiconductor interface," *Appl. Phys. Lett.*, vol. 87, 141101, October 3, 2005.

34. S.-J. Park, K.-F. Chen, S.-H. Sung, C. J. Wagner, and J. G. Eden, "Implications of microcavity plasma devices for new plasma display panel cell structures with improved luminosity," *J. Soc. Inf. Display*, vol. 13, no. 11, pp. 949-954, November 2005.

35. J. G. Eden and S.-J. Park, "Microcavity plasma devices and arrays: A new realm of plasma physics and photonic applications," *Plasma Phys. Control. Fusion*, vol. 47, pp. B83-B92, December 2005.

36. S.-J. Park, K.-S. Kim, and J. G. Eden, "Ultraviolet emission intensity, visible luminance, and electrical characteristics of small arrays of Al/Al_2O_3 microcavity plasma devices operating in Ar/N_2 or Ne at high power loadings," *J. Appl. Phys.*, vol. 99, 026107, January 15, 2006.

37. K.-F. Chen, N. P. Ostrom, S.-J. Park, and J. G. Eden, "One quarter million (500 × 500) pixel arrays of silicon microcavity plasma devices: Luminous efficacy above 6 lumens/watt

with Ne/50% Xe mixtures and a green phosphor," *Appl. Phys. Lett.*, vol. 88, 061121, February 6, 2006.

38. K. H. Becker, K. H. Schoenbach, and J. G. Eden, "Microplasmas and applications," *J. Phys. D: Appl. Phys.*, vol. 39, no. 3, pp. R55-R70, February 7, 2006 (Invited Topical Review).

39. J. G. Eden, "Information display early in the 21st century: Overview of selected emissive display technologies," *Proc. IEEE*, vol. 94, pp. 567-574, March 2006 (Invited).

40. C. J. Wagner and J. G. Eden, "Gerade Rydberg states of Xe_2 probed by laser spectroscopy in the afterglow of a Xe microplasma: $\Omega_g \leftarrow a^3\Sigma_u^+\left(1_u, O_u^-\right)$ transitions in the near-infrared (675-800 nm)," *Chem. Phys. Lett.*, vol. 422, pp. 372-377, May 10, 2006.

41. J. G. Eden, S.-J. Park, and K.-S. Kim, "Arrays of nonequilibrium plasmas confined to microcavities: An emerging frontier in plasma science and its applications," *Plasma Sources Sci. Technol.*, vol. 15, pp. S67-S73, May 2006 (Invited).

42. J. G. Eden and S.-J. Park, "New opportunities for plasma science in nonequilibrium, low temperature plasmas confined to microcavities: There's plenty of room at the bottom," *Phys. Plasmas*, vol. 13, 057101, May 2006 (Invited).

43. S.-J. Park, T. M. Spinka, and J. G. Eden, "Linear arrays of ceramic microcavity plasma devices (127-180 μm diameter) driven by buried coplanar electrodes: Shaping the intracavity electric field and emission profile," *Appl. Phys. Lett.*, vol. 89, 031502, July 17, 2006.

III. PATENTS

• PATENTS GRANTED UNDER AFOSR SUPPORT (2003-2006)

1. J. G. Eden, J. Gao, S.-J. Park, and C. J. Wagner, "High Pressure Arc Lamp Assisted Start Up Device and Method," U.S. Patent No. 6,541,915 (April 1, 2003).

2. B. A. Vojak, J. G. Eden, S.-J. Park, and C. J. Wagner, "Multilayer Ceramic Microdischarge Device," U.S. Patent No. 6,563,257 (May 13, 2003).

3. T. A. DeTemple, J. W. Frame, D. J. Wheeler, and J. G. Eden, "Microdischarge Lamp," Japanese Patent No. 3,455,234 (October 14, 2003).

4. J. G. Eden, S.-J. Park, and C. J. Wagner, "Microdischarge Devices and Arrays," U.S. Patent No. 6,695,664 (February 24, 2004).

5. J. G. Eden, S.-J. Park, and C. J. Wagner, "Method and Apparatus For Exciting a Microdischarge," U.S. Patent No. 6,815,891 (November 9, 2004).

6. J. G. Eden and S.-J. Park, "Microdischarge Photodetectors," U.S. Patent No. 6,828,730 (December 7, 2004).